Physics in Medicine & Biology

IPEM Institute of Physics and Engineering in Medicine

ACCEPTED MANUSCRIPT • OPEN ACCESS

Modulation transfer function (MTF) evaluation for x-ray phase imaging system employing attenuation masks

To cite this article before publication: Glafkos Havariyoun *et al* 2023 *Phys. Med. Biol.* in press https://doi.org/10.1088/1361-6560/acc927

Modulation Transfer Function (MTF) evaluation for x-ray phase imaging system employing attenuation masks

Glafkos Havariyoun, Lorenzo Massimi, Charlotte Hagen, Marco Endrizzi, Alessandro Olivo

Department of Medical Physics and Bioengineering, University College London, WC1E 6BT, UK

Corresponding Author:

Glafkos Havariyoun Email: glafcos.havariyoun.10@ucl.ac.uk

Abstract

Objective: Attenuation masks can be used in x-ray imaging systems to increase their inherent spatial resolution and/or make them sensitive to phase effects, a typical example being Edge Illumination X-ray phase contrast imaging (EI-XPCI). This work investigates the performance of a mask-based system such as EI-XPCI in terms of Modulation Transfer Function (MTF), in the absence of phase effects.

Approach: Pre-sampled MTF measurements, using an edge, were performed on the same system implemented without masks, with non-skipped masks and finally with skipped masks (i.e., masks in which apertures illuminate every other pixel row/column). Results are compared to simulations and finally images of a resolution bar pattern acquired with all the above setups are presented.

Main results: Compared to the detector's inherent MTF, the non-skipped mask setup provides improved MTF results. In comparison to an ideal case where signal spill-out into neighbouring pixels is negligible, this improvement takes place only at specific frequencies of the MTF, dictated by the spatial repetition of the spill-out signal. This is limited with skipped masks, which indeed provide further MTF improvements over a larger frequency range. Experimental MTF measurements are supported through simulation and resolution bar pattern images.

Significance: This work has quantified the improvement in MTF due to the use of attenuation masks and lays the foundation for how acceptance and routine quality control tests will have to be modified when systems using masks are introduced in clinical practice and how MTF results will compare to those of conventional imaging systems.

1. Introduction

Over recent decades, two (2D) and three dimensional (3D), i.e. tomographic, X-ray phase contrast imaging (XPCI) methods have indicated significant advantages over conventional

absorption X-ray imaging in the imaging of objects with small absorption differences against the background they are immersed in, especially in applications requiring high spatial resolution [1–4]. XPCI methods take advantage of the phase-shift effects caused by a sample (supplementary to the absorption effect), leading to an increase in contrast when compared to conventional X-ray imaging[5].

Edge illumination (EI) is a non-interferometric XPCI technique that has been successfully implemented with both synchrotron and conventional laboratory sources[6–8]. The method has been extended to quantitative computed tomography (CT) and has more recently successfully demonstrated its capabilities in biological tissue imaging using a compact version of the system[9–12]. It has proven its ability to provide reliable quantitative results with spatially and temporally incoherent X-ray sources, reduced exposure times, higher X-ray energies, relatively flexible setup requirements and large fields of view (FOV)[13–15].

Figure 1 illustrates a schematic of the laboratory-based implementation of EI XPCI. Relative to a conventional X-ray imaging system the setup differs only in the introduction of two masks, made of a series of alternating apertures and absorbing septa, between the source and the detector.

The sample mask, placed before the sample, creates a series of secondary beamlets each of which propagates towards a single pixel detector column. The detector mask, aligned with the detector pixels, blocks a pre-determined fraction of each beamlet – effectively creating insensitive regions between adjacent pixels. Placement of a sample between the two masks has two effects: attenuation of the beamlet intensity and beam refraction i.e., a local change in the beam's direction of propagation.

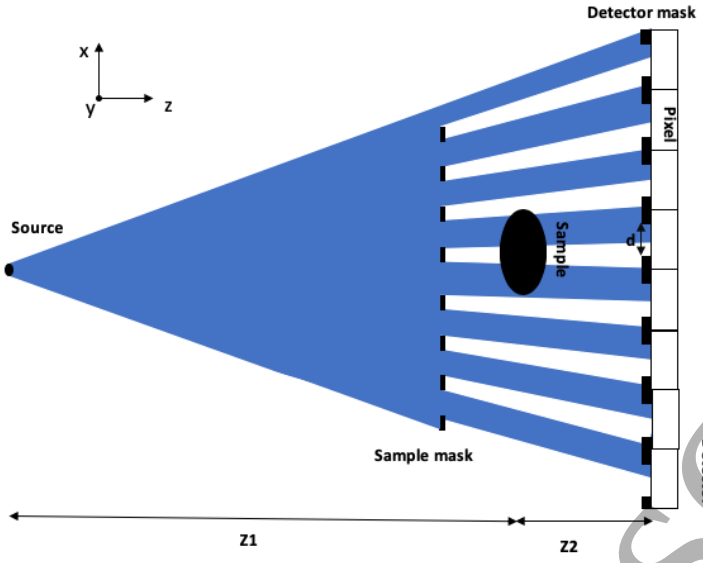

a)

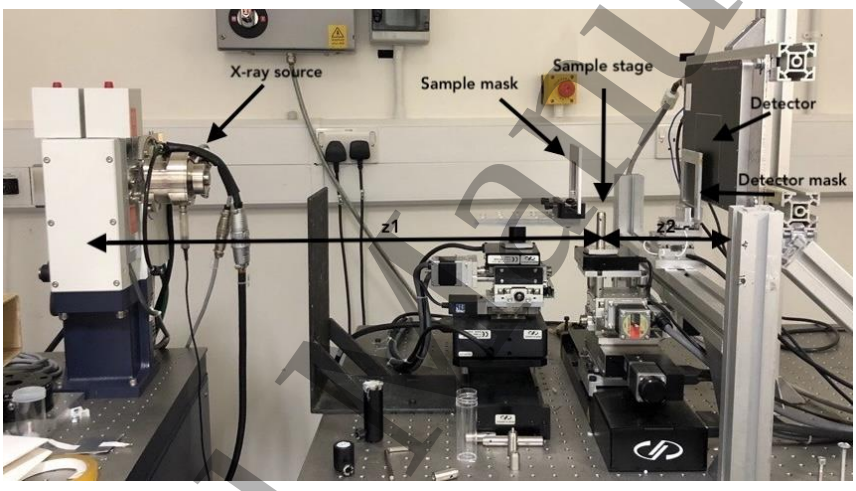

b)

Figure 1. a) Schematic diagram (top view, not to scale) of the EI setup with a laboratory X-ray source.The source to sample distance (Z1) is 70cm and the sample to detector distance (Z2) is 15cm. b) A photo of the phase contrast edge illumination setup currently in use at UCL.

Lateral misalignment of the two masks (along x in Fig 1) allows for: a change in the detected intensity of the beamlets and a variation of the refraction sensitivity of the system[16]. A process called "dithering", where multiple frames are acquired whilst the sample is shifted by sub-pixel steps, is often used to further improve resolution and accuracy of the retrieved quantitative information [17,18]. The optimal number of dithering steps depends on the source size, sample mask slit width and sample structures [19]; for a correct recombination, the size of the dithering step needs to be a submultiple of the sample mask period. The ultimate attainable resolution is equal to the aperture size; if such a maximum resolution is targeted,

compliance with the Nyquist-Shannon theorem requires a dithering step of half the aperture size. Higher resolution images obtained by recombining frames obtained through dithering can suffer from artefacts if a detector with a line spread function (LSF) significantly greater than a pixel, described as “signal spill out” or “signal diffusion”, is used. “Skipped” masks, where every other detector column is illuminated, can be implemented in these cases to mitigate the problem; in such a setup, data from skipped pixel columns are “dumped”[20]. For a more detailed explanation of the method’s principles and how phase effects are exploited, the reader is referred to a recent review[15].

To fully characterize the performance of an imaging system several key characteristics, some specific to XPCI, need to be investigated. Previous work on the EI technique has investigated angular resolution, sensitivity, spatial resolution, contrast and noise properties[19,21–24]. However, the modulation transfer function (MTF), commonly used in conventional X-ray imaging systems to characterize their spatial frequency response[25], has not yet been studied. While the MTF and PSF of some of the detectors used in EI setups have been investigated in previous studies, there has been no previous work on, and comparison of, the effect of the different mask types on the MTF[26,27]. Previous work has either been limited to simulations or has only reported on experimentally measured Edge Spread Functions (ESFs)[10,17,19]. MTF evaluation is a key characterisation procedure that forms part of the acceptance tests of digital X-ray imaging devices as per the International Electrotechnical Commission’s (IEC) standards (IEC 62220-1-1:2015) as well as routine medical physics tests performed for quality control and beyond[28]. The MTF is significantly altered by the introduction of the masks, hence we found it needed to be discussed in detail before mask-based XPCI could be translated to clinical practice. To the best of our knowledge, MTF evaluation of other XPCI systems have focused on CT systems[29] apart from one work which involved simulated results for 2D in-line phase contrast imaging[30]. In this work, we evaluate via simulations and experiments the pre-sampled MTF of EI, and how this affects the resolution of the system. The response of a digital imaging system with discrete sampling does not only depend on the properties of the detector but also on the input signal and its location relative to the sampling grid of the detector. To avoid aliasing effects caused by the discrete sampling of the input signal the edge is angled to increase the effective sampling rate and obtain a non aliased response, pre-sampled (i.e. effectively sampled at a frequency higher than the pixel pitch) MTF[31,32]. The

relevance of this work goes beyond EI XPCI and is more generally applicable to methods using pre-sample masks, either to gain access to some degree of phase-based image contrast or specifically to increase the resolution [33–36].

2. Materials and Methods

The source used was a Rigaku Micro-Max 007 rotating anode (Rigaku Corporation, Japan) with a molybdenum anode and an effective focal spot size of approximately 70 µm. The detector was a CMOS-based flat panel C9732DK-11 (Hamamatsu, Japan) with directly deposited CsI and a 50 by 50 µm pixel size (pixel pitch (p) of 50 µm) with a PSF with an approximately 100 µm Full Width Half Maximum (FWHM)[27]. The source to detector distance is 85 cm, while the source to sample distance is 70 cm.

Images were acquired without masks, with non-skipped masks and finally with skipped masks. For the non-skipped masks, the aperture size/period were 12 µm/38 µm and 20 µm/48 µm for the sample and detector mask, respectively. For the skipped masks, the same quantities were 10 µm/79 µm and 17 µm/98 µm, respectively. The masks have been manufactured by Microworks GmbH (Karlshrue, Germany) and are made by gold electroplating on a 400 µm thick graphite substrate. The thickness of the gold layer is > 120µm from specifications. Dithering was performed in the skipped masked acquisitions to match the pixel size of the non-dithered, non-skipped mask acquisition.

The source was operated at 40 kVp for all acquisitions. A 45 µm Molybdenum filter, commonly used in breast imaging X-ray systems, was added in front of the source for the no-masks acquisitions to prevent detector saturation. Acquisitions with the non-skipped mask setup were performed both with and without the additional filtration to allow for a direct comparison (in terms of beam hardness) with the no-masks and skipped masks setups, respectively. Phase retrieval was not performed on the images. The scope of this work is to establish how the introduction of (skipped and non-skipped) attenuation masks affects the detector's response in terms of input and output signal in the spatial frequency domain; e.g., it should be noted that a phase-contrast image simply has a different distribution of spatial frequencies compared to an attenuation one, and these individual frequencies would be transferred through the system according to the same MTF. As an overall system parameter,

it is inherently related to the point spread function (PSF) of the detector, x-ray source size and, for the EI-XPCI system, attenuation masks. Furthermore, masks can be added also to increase the spatial resolution of an imaging system, which makes the presented results also relevant to some non-XPCI areas[37]. All images acquired were dark noise and flat field corrected.

Images were acquired with a 1 mm thick tungsten edge at a slight angulation (1.5°-2°). Due to the presence of the detector masks, the edge cannot be placed in contact with the detector in cases where the masks were employed. Hence, the edge was placed at the usual sample position of the system for all acquisitions. It is known that MTF measurements are affected by geometry parameters and source blurring. However, as all measurements were taken with the edge at the same position and magnification was considered when calculating pre-sampled MTFs, this allowed a fair comparison among the three setups. Note that this resulted in all presented graphs being referred to the (de-magnified) sample coordinates. Transmission through the edge was measured to be below <2% for all setups. To obtain the pre-sampled MTF, an oversampled edge spread function (ESF) approach was implemented[25]. The ESF was smoothed with a median filter (window size of 5); according to reference [31], window sizes up to 17 can be used with median filtering to reduce noise in the tails while preserving as much as possible the integrity of the data [31]. Furthermore, a median filter of length 5 pixels is routinely used by the UK's National Health Screening (NHS) Breast Screening Programme for MTF evaluation[38]. The ESF was then differentiated to obtain the line spread function (LSF), which in turn was Fourier transformed to obtain the pre-sampled MTF. Finally, a Hüttner Type 18UL resolution lead (0.03mm thickness) bar pattern with line pairs ranging from 1 lp/mm to 20 lp/mm was imaged under the same conditions as the edge for a qualitative evaluation.

Simulations were performed using a wave optics simulation of the EI setup[39]. The edge shape was modelled as a step function considering the attenuation and refractive properties of tungsten. As the simulation involves a one-dimensional representation of the setup (i.e., single detector row) oversampled ESFs were obtained by dithering the simulated edge. As dithering was also employed experimentally, it was possible to obtain measured pre-sampled MTFs using this same method for comparison. It should be noted that this method provides

a more accurate ESF, and therefore pre-sampled MTF results, because it eliminates the need to determine the edge angle and the perpendicular distances from the edge to the centre of each pixel.

3. Results and Discussion

3.1 Effect of non-skipped masks

Figure 2 shows the experimentally acquired tungsten edge images from which the LSFs and MTFs (in the horizontal direction, i.e., perpendicular to mask apertures) displayed in Figure 3 were obtained. Note that the signal spill out effect of the detector is made evident by the gradual grey level change of the edge on the mask-less image (Figure 2a). The red arrows on the non-skipped mask image (Figure 2b) indicate the appearance of step like effects. These can be explained by the introduction of the masks producing insensitive regions on the detector, hence causing a reduction in the width of the detector's PSF.

a) b)

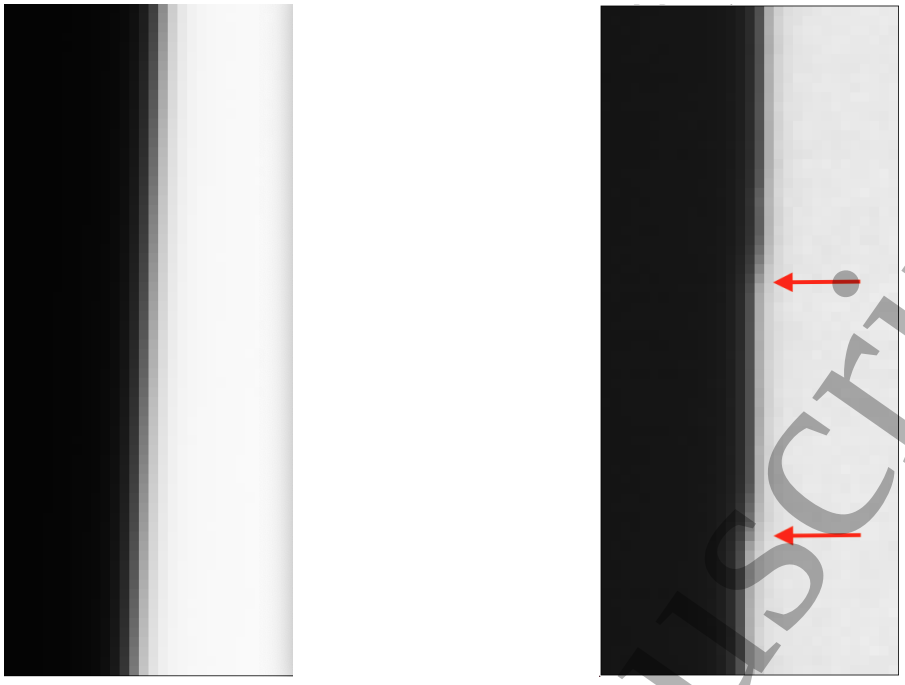

Figure 2: Images of a tungsten edge obtained with: a) no masks and b) with non-skipped masks on the EI XPCI system. Red arrows on (b) indicate a step-like effect not present in (a). Images displayed with identical windowing (255) and levelling (128).

Figure 3 shows the experimental LSFs (Figure 3a) and MTFs (Figure 3b) obtained for the mask-less and non-skipped mask setups. Although the envelope of the LSF does not change, we notice the presence of secondary "lobes", caused by the step like effects highlighted in Figure 2b, at higher spatial distances in the latter case. The number of lobes introduced is dependent on the intrinsic signal "spill-out" (i.e., the width of the LSF) of the used detector. For the Hamamatsu detector, this was previously reported to be 49% and 6% to the first and second neighbouring pixel if only one pixel was illuminated[40]. The secondary lobes repeat in space; their FWHM matches the sample mask's aperture and the spacing between the lobes is equal to the pixel pitch (p). This effectively corresponds to a convolution of the detector LSF without the mask with a comb function with period equal to p. When this is Fourier-transformed to obtain the MTF curve (Figure 3b), this results in a sampling effect with period 1/p on the broader MTF corresponding to the narrow, aperture-driven LSF. This leads to a suppression of this MTF curve at frequencies that do not match the 1/p sampling period.

a) b)

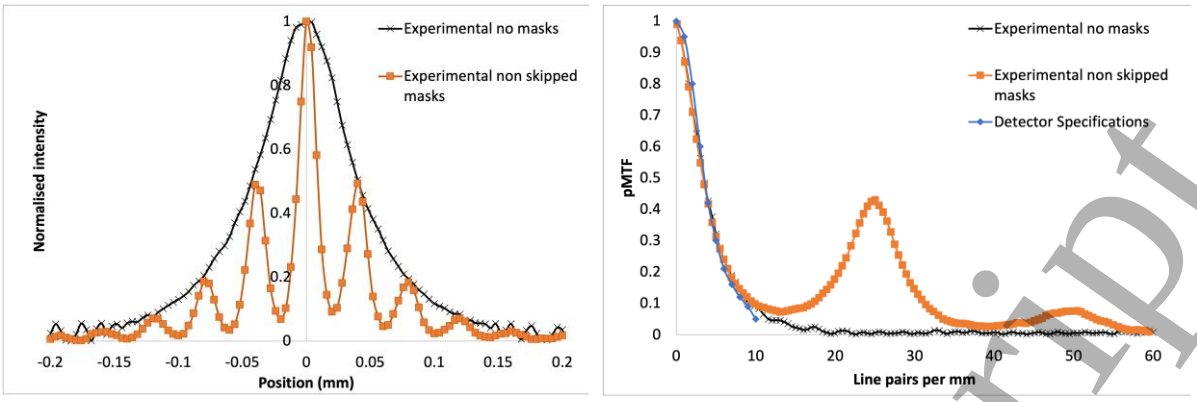

Figure 3: a) Line Spread Functions (LSFs) and b) Modulation Transfer Functions (MTF) of the EI XPCI setup with and without non-skipped masks. Data were obtained through a tungsten edge in the plane perpendicular to mask apertures. The blue line on the MTF graph displays the manufacturer's MTF for the C9732DK-11 (Hamamatsu, Japan) detector.

This is further demonstrated by the simulation results displayed in Figure 4. The simulation confirms the introduction of secondary lobes on the LSF (Figure 4a) when non-skipped masks are used, the intensity and number of which depend on the width of the original LSF. The simulated MTF results (Figure 4b) also support the experimental results, with additional lobes appearing with frequency 1/p. Results also indicate that if all the secondary lobes were to be removed from the LSF (i.e. removing all the signal spill-out), leaving only the central one, an MTF corresponding to the Fourier transform of the narrower, aperture-driven LSF would be obtained, with a smooth curve at high frequencies and no lobes. Indeed, removing all secondary lobes corresponds to an "infinite" repetition frequency of the narrow LSF, and therefore to a perfectly sampled MTF. This indicates that the use of skipped masks, where only every other column is illuminated, should increase the sampling frequency of the MTF by a factor of two, leading to a better overall frequency response.

a) b)

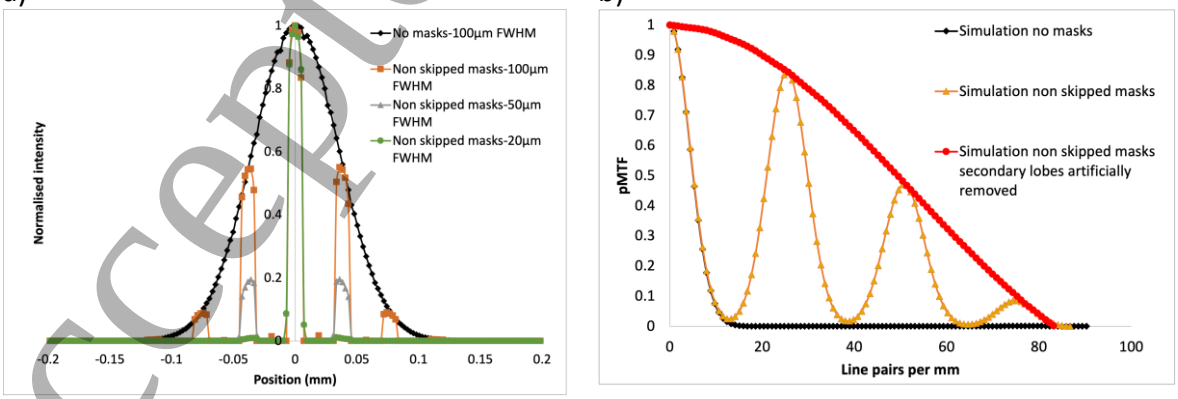

Figure 4: a) Simulated Line Spread Functions with various detector Point Spread Functions/Full Width Half Maximum and b) Simulated Modulation Transfer Functions of

the EI XPCI setup with and without non-skipped masks obtained by implementing the same tunsten edge method. The red MTF curve (small circular markers) indicate the predicted MTF curve if the secondary lobes from the LSFs were artifically removed.

It should be noted that the discrepancy in terms of number and intensity of the lobes (e.g., the second lobe having a peak value of 0.2 (Figure 3a) instead of the expected 0.06 based on the detector's specifications) between simulations and experimental results (Figures 3 and 4) is due to the difference in how the oversampled ESF was obtained in the two cases, i.e., slanted edge versus single row dithered edge respectively. Figure 5 shows the results obtained using both methods. Retrieving the ESF from a single pixel row of a dithered acquisition (10 dithering steps) provides results very close to the simulation (Figure 5a) and to the results expected from the detector's specifications (the second lobe's peak value is now close to the expected one of 6%). Conversely, retrieving the ESF using the slanted edge method and multiple pixel rows leads to a broadening of the lobes and to a non-zero intensity between them. This can be attributed to a number of factors including but not limited to the additional inaccuracies in estimating the angle and position of edge transitions (in turn caused by the step effects on the edge images), to small variations in the sensitivities of individual pixel columns and to small mask misalignments.

a) b)

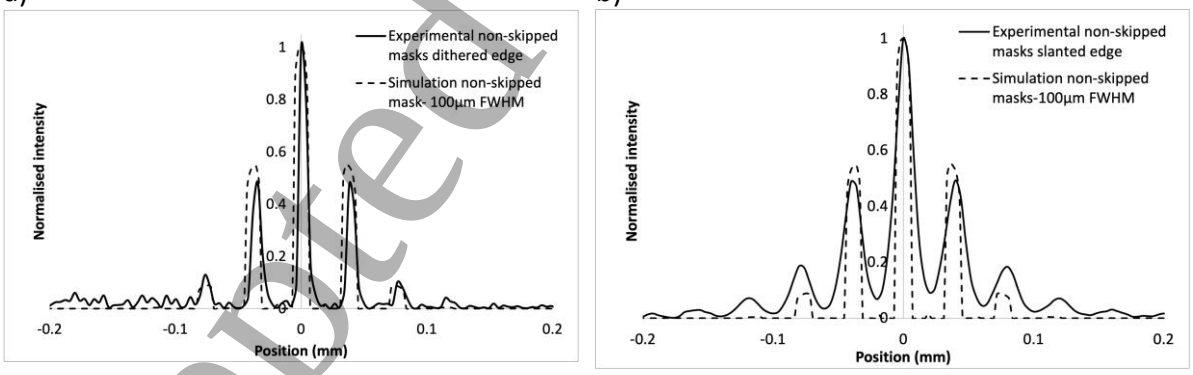

Figure 5: Experimental and simulated Line Spread Functions of the EI XPCI setup with non-skipped masks in the plane perpendicular to mask apertures. Simulated LSF results are compared to experimental results obtained from: a) a single image row of a dithered image (10 dithering steps) and b) using the standard slanted edge method.

3.2 Effect of skipped masks

Figure 6 depicts LSF (left) and pre-sampled MTF results (right) for the non-skipped and skipped masks. Note that the skipped-masks image was acquired with 2 dithering steps to achieve the same pixel size as a non-dithered non-skipped mask acquisition. The secondary lobes on the LSF (Figure 6a) due to signal spill-out into the first neighbour are no longer present when using the skipped masks, as every other pixel column is masked completely and the corresponding data is dumped. The third lobe, however, is still present, as the second neighbour is not covered and this still receives some degree of signal sharing occurring from the nearest "unmasked" pixel columns. As anticipated, this leads to significantly heightened MTF values (Figure 6b) at values midway through the lobes previously observed for the non-skipped case, confirming a doubling of the frequencies at which the MTF is correctly reproduced (i.e. with lobes appearing every 1/(2p) as opposed to 1/p). Since tertiary lobes (signal spillage into second neighbouring pixel columns) are still present, there is still a degree of spatial repetition of the "narrow" LSF, meaning that the "ideal" red curve shown in Figure 4b is still not obtained; in order to obtain such an MTF curve, all signal spill-out should be eliminated. However, as it can be seen the presence of only the (less intense) tertiary lobes in the spatial domain has led to a smaller suppression of the pMTF in the spatial frequency domain.

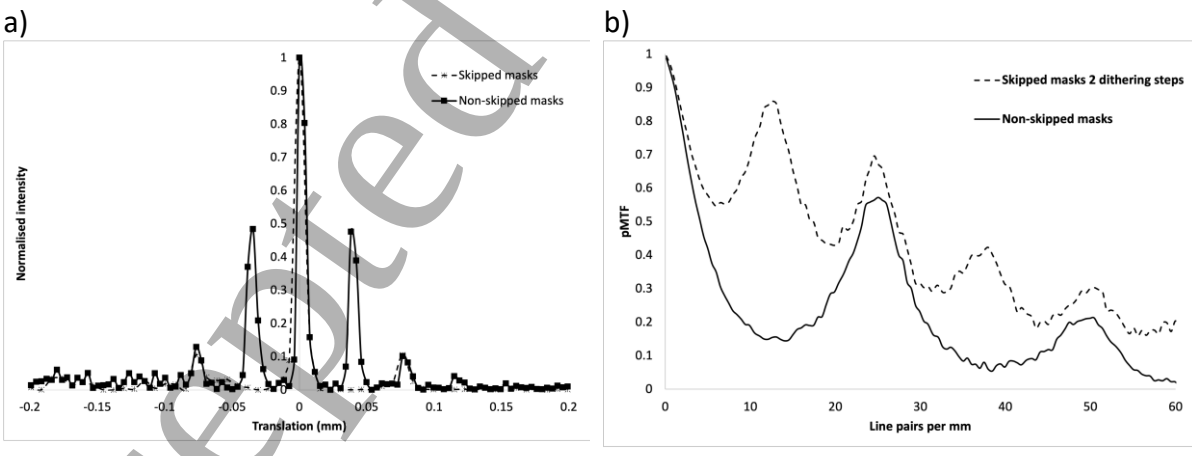

Figure 6: a) Line Spread Functions (LSFs) and b) Modulation Transfer Functions (MTF) of the EI XPCI setup with non-skipped (continuous lines) and skipped masks (dashed lines) obtained with a tungsten edge in the plane perpendicular to the mask apertures.

3.3 Effect on resolution

Figure 7 shows images of the bar phantom imaged with the EI setup with no masks (Figure 7a), non-skipped masks (Figure 7b) and skipped-masks (Figure 7c). Also in this case, two dithering steps were used in the skipped-mask case to obtain the same pixel size as in the other two setups. The three bar groups visible in the images are, from left to right, 8.9, 12.5 and 16.6 lp/mm, respectively. The improvement in resolution from left to right is evident. This is expected based on the LSF and MTF results shown previously. Attention should be given to the 12.5 lp/mm (central) group: the non-skipped image (Figure 7b) shows some improvement at this frequency when compared to the no-masks case (Figure 7a), but the change is much more significant in the skipped-mask image (Figure 7c).

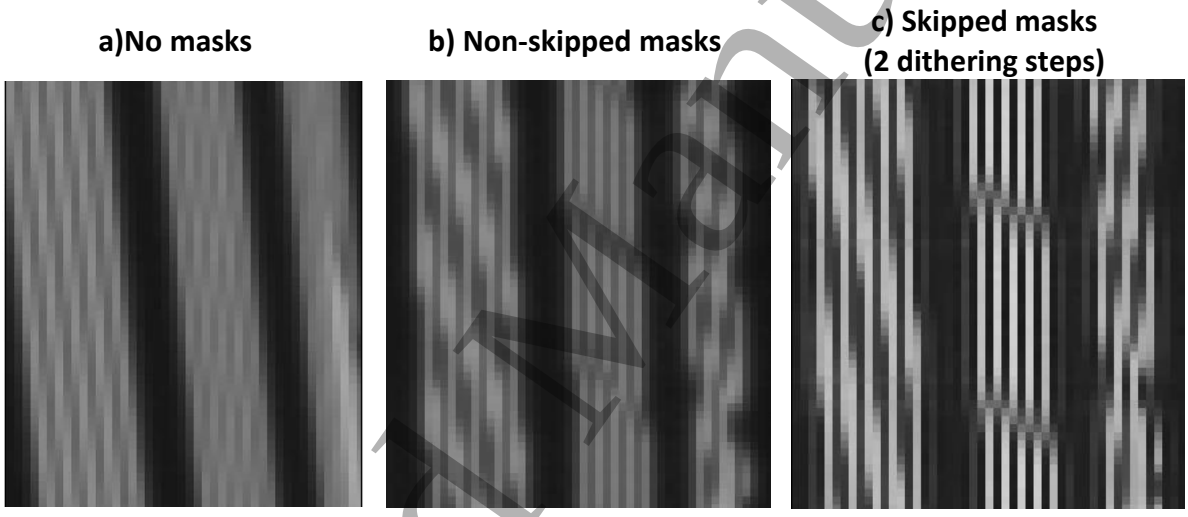

Figure 7: Hüttner Type 18UL resolution lead (0.03mm thickness) bar pattern images (same grayscale and windowing (255) and levelling (128)) obtained with the EI XPCI system with: a) no masks, b) non-skipped masks, c) skipped-masks. From left to right the line groups have a spatial frequency of 8.9, 12.5 and 16.6 lp/mm, respectively.

This should be expected as 12.5 lp/mm is one of the "supressed" frequencies in the non-skipped mask case which is recovered in the skipped case, as visible in Figure 7c. Furthermore, although there is an improvement compared to the no-masks and non-skipped masks cases, the suppression of frequencies both above and below 12.5 lp/mm (i.e. at 8.9 lp/mm and 16.6 lp/mm) is clearly visible in the skipped masked acquisition. Again, this could be expected from the MTF curve for this setup (Figure 7b). The effects of aliasing, light and dark bands with varying spacing and orientation to the bar patterns, can be seen in all images[41]. The change

in orientation of the bands occurs between the first- and second-line pair groups in the image acquired without masks and between the second and third line pair groups in the images acquired with both masks. The spacing of the aliasing patterns increase from Figure 7a to Figure 7c. Both these effects are a consequence of the increase in sampling frequency discussed above and of the effective change in resolution of the detector due to the introduction of the sample masks. We also note that the smaller aperture and larger period of the sample and detector skipped masks (i.e. less photons reaching the sample and detector) means there is trade off between increased resolution and exposure time. The resulting increase in exposure time can only be overcome by utilising a higher flux X-ray source. This, however, does not translate into a dose increase, since the mask is placed upstream of the imaged sample, an aspect discussed in detail in previous work [42,43]. The choice between non-skipped and skipped masks depends primarily on whether the used detector has a significant or negligible signal spill-out: skipped masks are needed in the former case, while non-skipped ones can be used in the latter. If the same resolution level (as determined by the size of the pre-sample aperture[19]) is desired, then the use of skipped masks will require double the exposure time.

4 Conclusions

Simulation and experimental results of the LSF and MTF of the EI-XPCI setup have been presented for the non-skipped and skipped mask setups and further supported with images of a resolution bar pattern. It has been shown that the introduction of masks leads to an improvement in MTF and hence spatial resolution and contrast transfer function of the system. The introduction of the masks, specifically the sample mask, introduces a selective improvement in MTF performance driven by the sample mask aperture size and pixel pitch p. The use of skipped masks doubles the improvement in MTF in terms of frequencies being correctly reproduced. This work has led to further understanding of the impact of sample mask aperture size, pitch and detector PSF in terms of spatial frequency response of the EI XPCI system. In particular, it has shown how signal spill-out and the consequent creation of spurious peaks in the LSF leads to the suppression of certain spatial frequencies in the MTF, and how these can be partially restored by reducing the impact of signal spill-out through skipped mask designs.

This can be used in future experiments to identify the most appropriate system properties for the imaging task in hand; for example, by making sure that the imaging system is sensitive in a given range of spatial frequencies, which in turn can be important for the correct reproduction of certain object features. Furthermore, in the light of a future clinical adoption of EI XPCI, this work lays the foundation for how acceptance and routine quality controls tests will have to be modified, and how results will compare to conventional systems. As made clear by e.g. Figure 4b, the MTF of a system employing masks looks very different from that of a system that does not; the same figure provides both a direct comparison with a system using the same detector with no masks, and the "ideal" MTF the system with masks could aspire to if all spill-out effects were eliminated: in practical terms, the MTF of a system with masks will always lie between these two extremes.

Acknowledgements

This work was supported by Engineering and Physical Sciences Research Council (EPSRC) (Grant EP/T005408/1). A.O. is supported by the Royal Academy of Engineering under their Chairs in Emerging Technologies scheme (Grant CiET1819/2/78).

References

1. Mayo S, Endrizzi M. X-Ray Phase Contrast Methods. In: Ida N, Meyendorf N, eds. *Handbook of Advanced Nondestructive Evaluation*. Springer International Publishing; 2019:1053-1093. doi:10.1007/978-3-319-26553-7_54

2. Bravin A, Coan P, Suortti P. X-ray phase-contrast imaging: from pre-clinical applications towards clinics. *Phys Med Biol*. 2012;58(1):R1-R35. doi:10.1088/0031-9155/58/1/R1

3. Momose A. X-ray phase imaging reaching clinical uses. *Physica Medica*. 2020;79:93-102. doi:10.1016/j.ejmp.2020.11.003

4. Hagen CK, Diemoz PC, Olivo A. On the relative performance of edge illumination x-ray phase-contrast CT and conventional, attenuation-based CT. *Medical Physics*. 2017;44(5):1876-1885. doi:10.1002/mp.12179

5. Olivo A, Castelli E. X-ray phase contrast imaging: From synchrotrons to conventional sources. *Riv Nuovo Cim*. 2014;37(9):467-508. doi:10.1393/ncr/i2014-10104-8

6. Olivo A, Speller R. A coded-aperture technique allowing x-ray phase contrast imaging with conventional sources. *Appl Phys Lett*. 2007;91(7):074106. doi:10.1063/1.2772193

7. Munro PRT, Ignatyev K, Speller RD, Olivo A. Phase and absorption retrieval using incoherent X-ray sources. *PNAS*. 2012;109(35):13922-13927. doi:10.1073/pnas.1205396109

8. Diemoz PC, Endrizzi M, Zapata CE, et al. X-Ray Phase-Contrast Imaging with Nanoradian Angular Resolution. *Phys Rev Lett*. 2013;110(13):138105. doi:10.1103/PhysRevLett.110.138105

9. Hagen CK, Diemoz PC, Endrizzi M, et al. Quantitative edge illumination x-ray phase contrast tomography. In: *Developments in X-Ray Tomography IX*. Vol 9212. International Society for Optics and Photonics; 2014:921205. doi:10.1117/12.2061322

10. Massimi L, Suaris T, Hagen CK, et al. Volumetric high-resolution X-ray phase-contrast virtual histology of breast specimens with a compact laboratory system. *IEEE Transactions on Medical Imaging*. Published online 2021:1-1. doi:10.1109/TMI.2021.3137964

11. Massimi L, Suaris T, Hagen CK, et al. Detection of involved margins in breast specimens with X-ray phase-contrast computed tomography. *Sci Rep*. 2021;11(1):3663. doi:10.1038/s41598-021-83330-w

12. Havariyoun G, Vittoria FA, Hagen CK, et al. A compact system for intraoperative specimen imaging based on edge illumination x-ray phase contrast. *Phys Med Biol*. 2019;64(23):235005. doi:10.1088/1361-6560/ab4912

13. Endrizzi M, Basta D, Olivo A. Laboratory-based X-ray phase-contrast imaging with misaligned optical elements. *Appl Phys Lett*. 2015;107(12):124103. doi:10.1063/1.4931778

14. Astolfo A, Endrizzi M, Vittoria FA, et al. Large field of view, fast and low dose multimodal phase-contrast imaging at high x-ray energy. *Scientific Reports*. 2017;7(1):2187. doi:10.1038/s41598-017-02412-w

15. Olivo A. Edge-illumination x-ray phase-contrast imaging. *J Phys: Condens Matter*. 2021;33(36):363002. doi:10.1088/1361-648X/ac0e6e

16. Olivo A, Speller R. A coded-aperture technique allowing x-ray phase contrast imaging with conventional sources. *Appl Phys Lett*. 2007;91(7):074106. doi:10.1063/1.2772193

17. Diemoz PC, Endrizzi M, Hagen CK, Millard TP, Vittoria FA, Olivo A. Angular sensitivity and spatial resolution in edge illumination X-ray phase-contrast imaging. *Nuclear Instruments and Methods in Physics Research Section A: Accelerators, Spectrometers, Detectors and Associated Equipment*. 2015;784:538-541. doi:10.1016/j.nima.2014.12.027

18. Hagen CK, Diemoz PC, Endrizzi M, Olivo A. The effect of the spatial sampling rate on quantitative phase information extracted from planar and tomographic edge illumination x-ray phase contrast images. *J Phys D: Appl Phys*. 2014;47.

19. Diemoz PC, Vittoria FA, Olivo A. Spatial resolution of edge illumination X-ray phase-contrast imaging. *Opt Express, OE*. 2014;22(13):15514-15529. doi:10.1364/OE.22.015514

20. Ignatyev K, Munro PRT, Speller RD, Olivo A. Effects of signal diffusion on x-ray phase contrast images. *Review of Scientific Instruments*. 2011;82(7):073702. doi:10.1063/1.3606442

21. Diemoz PC, Endrizzi M, Zapata CE, et al. X-Ray Phase-Contrast Imaging with Nanoradian Angular Resolution. *Phys Rev Lett*. 2013;110(13):138105. doi:10.1103/PhysRevLett.110.138105

22. Diemoz PC, Hagen CK, Endrizzi M, Olivo A. Sensitivity of laboratory based implementations of edge illumination X-ray phase-contrast imaging. *Applied Physics Letters*. 2013;103. Accessed February 18, 2019. http://dx.doi.org/10.1063/1.4845015

23. Diemoz PC, Vittoria FA, Olivo A. Concept of contrast transfer function for edge illumination x-ray phase-contrast imaging and its comparison with the free-space propagation technique. *Opt Express, OE*. 2016;24(10):11250-11265. doi:10.1364/OE.24.011250

24. Hagen CK, Roche i Morgó O, Olivo A. Predicting the noise in hybrid (phase and attenuation) x-ray images acquired with the edge illumination technique. *Medical Physics*. 2020;47(9):4439-4449. doi:10.1002/mp.14366

25. Samei E, Flynn MJ, Reimann DA. A method for measuring the presampled MTF of digital radiographic systems using an edge test device. *Med Phys*. 1998;25(1):102-113. doi:10.1118/1.598165

26. Konstantinidis AC, Zheng Y, Olivo A, et al. Evaluation of a novel wafer-scale CMOS APS X-ray detector for use in mammography. In: *2012 IEEE Nuclear Science Symposium and Medical Imaging Conference Record (NSS/MIC)*. ; 2012:3254-3260. doi:10.1109/NSSMIC.2012.6551742

27. Endrizzi M, Oliva P, Golosio B, Delogu P. CMOS APS detector characterization for quantitative X-ray imaging. *Nuclear Instruments and Methods in Physics Research Section A: Accelerators, Spectrometers, Detectors and Associated Equipment*. 2013;703:26-32. doi:10.1016/j.nima.2012.11.080

28. IPEM. *Report 32 Part VII (1st Edition) Measurement of the Performance Characteristics of Diagnostic X-Ray Systems: Digital Imaging Systems*. IPEM; 2010. Accessed March 3, 2023. https://www.ipem.ac.uk/resources/books/report-32-part-vii-1st-edition-digital-imaging-systems/

29. Li K, Zambelli J, Bevins N, Ge Y, Chen GH. Spatial resolution characterization of differential phase contrast CT systems via modulation transfer function (MTF) measurements. *Phys Med Biol*. 2013;58(12):4119-4135. doi:10.1088/0031-9155/58/12/4119

30. Sun X, Gao F, Zhao H, Zhang L, Li J, Zhou Z. MTF evaluation of in-line phase contrast imaging system. In: *Quantitative Phase Imaging III*. Vol 10074. SPIE; 2017:120-127. doi:10.1117/12.2250480

31. M D, D Z, H L. Step by step analysis toward optimal MTF algorithm using an edge test device. *Journal of X-ray science and technology*. 2009;17(1). doi:10.3233/XST-2009-0210

32. IEC. IEC 62220-1-1:2015 |Medical electrical equipment - Characteristics of digital X-ray imaging devices - Part 1-1: Determination of the detective quantum efficiency - Detectors used in radiographic imaging. Accessed March 3, 2023. https://webstore.iec.ch/publication/21937

33. Krejci F, Jakubek J, Kroupa M. Hard x-ray phase contrast imaging using single absorption grating and hybrid semiconductor pixel detector. *Review of Scientific Instruments*. 2010;81(11):113702. doi:10.1063/1.3499372

34. Dreier ES, Silvestre C, Kehres J, et al. Virtual subpixel approach for single-mask phase-contrast imaging using Timepix3. *J Inst*. 2019;14(01):C01011-C01011. doi:10.1088/1748-0221/14/01/C01011

35. Wen H, Gomella AA, Patel A, et al. Subnanoradian X-ray phase-contrast imaging using a far-field interferometer of nanometric phase gratings. *Nat Commun*. 2013;4:2659. doi:10.1038/ncomms3659

36. Roche I Morgó O, Vittoria F, Endrizzi M, Olivo A, Hagen CK. Technical Note: Practical implementation strategies of cycloidal computed tomography. *Med Phys*. 2021;48(10):6524-6530. doi:10.1002/mp.14821

37. Hagen CK, Vittoria FA, Morgó OR i, Endrizzi M, Olivo A. Cycloidal Computed Tomography. *Phys Rev Applied*. 2020;14(1):014069. doi:10.1103/PhysRevApplied.14.014069

38. Marshall N. Calculation of Quantitative Image Quality Parameters. Published online 2009. Accessed March 1, 2023. https://assets.publishing.service.gov.uk/government/uploads/system/uploads/attachment_data/file/442798/nhsbsp-equipment-report-0902.pdf

39. Vittoria FA, Diemoz PC, Endrizzi M, et al. Strategies for efficient and fast wave optics simulation of coded-aperture and other x-ray phase-contrast imaging methods. *Appl Opt*. 2013;52(28):6940-6947. doi:10.1364/AO.52.006940

40. Olivo A, Ignatyev K, Munro PRT, Speller RD. Design and realization of a coded-aperture based X-ray phase contrast imaging for homeland security applications. *Nuclear Instruments and Methods in Physics Research Section A: Accelerators, Spectrometers,*

Detectors and Associated Equipment. 2009;610(2):604-614. doi:10.1016/j.nima.2009.08.085

41. Albert M, Beideck DJ, Bakic PR, Maidment ADA. Aliasing effects in digital images of line-pair phantoms. *Med Phys*. 2002;29(8):1716-1718. doi:10.1118/1.1493212

42. Hagen CK, Munro PRT, Endrizzi M, Diemoz PC, Olivo A. Low-dose phase contrast tomography with conventional x-ray sources. *Med Phys*. 2014;41(7):070701. doi:10.1118/1.4884297

43. Olivo A, Gkoumas S, Endrizzi M, et al. Low-dose phase contrast mammography with conventional x-ray sources. *Medical Physics*. 2013;40(9):090701. doi:10.1118/1.4817480